# First model-independent determination of the relative strong phase between $D^0$ and $\bar{D}^0 \to K_S^0 \pi^+ \pi^-$ and its impact on the CKM angle $\gamma/\phi_3$ measurement

R. A. Briere,[1] H. Vogel,[1] P. U. E. Onyisi,[2] J. L. Rosner,[2] J. P. Alexander,[3] D. G. Cassel,[3] J. E. Duboscq,[3,*] R. Ehrlich,[3] L. Fields,[3] L. Gibbons,[3] R. Gray,[3] S. W. Gray,[3] D. L. Hartill,[3] B. K. Heltsley,[3] D. Hertz,[3] J. M. Hunt,[3] J. Kandaswamy,[3] D. L. Kreinick,[3] V. E. Kuznetsov,[3] J. Ledoux,[3] H. Mahlke-Krüger,[3] D. Mohapatra,[3] J. R. Patterson,[3] D. Peterson,[3] D. Riley,[3] A. Ryd,[3] A. J. Sadoff,[3] X. Shi,[3] S. Stroiney,[3] W. M. Sun,[3] T. Wilksen,[3] S. B. Athar,[4] J. Yelton,[4] P. Rubin,[5] S. Mehrabyan,[6] N. Lowrey,[6] M. Selen,[6] E. J. White,[6] J. Wiss,[6] R. E. Mitchell,[7] M. R. Shepherd,[7] D. Besson,[8] T. K. Pedlar,[9] D. Cronin-Hennessy,[10] K. Y. Gao,[10] J. Hietala,[10] Y. Kubota,[10] T. Klein,[10] R. Poling,[10] A. W. Scott,[10] P. Zweber,[10] S. Dobbs,[11] Z. Metreveli,[11] K. K. Seth,[11] B. J. Y. Tan,[11] A. Tomaradze,[11] J. Libby,[12] L. Martin,[12] A. Powell,[12] G. Wilkinson,[12] H. Mendez,[13] J. Y. Ge,[14] D. H. Miller,[14] V. Pavlunin,[14] B. Sanghi,[14] I. P. J. Shipsey,[14] B. Xin,[14] G. S. Adams,[15] D. Hu,[15] B. Moziak,[15] J. Napolitano,[15] K. M. Ecklund,[16] Q. He,[17] J. Insler,[17] H. Muramatsu,[17] C. S. Park,[17] E. H. Thorndike,[17] F. Yang,[17] M. Artuso,[18] S. Blusk,[18] N. Horwitz,[18] S. Khalil,[18] J. Li,[18] R. Mountain,[18] K. Randrianarivony,[18] N. Sultana,[18] T. Skwarnicki,[18] S. Stone,[18] J. C. Wang,[18] L. M. Zhang,[18] G. Bonvicini,[19] D. Cinabro,[19] M. Dubrovin,[19] A. Lincoln,[19] P. Zhou,[19] J. Zhu,[19] P. Naik,[20] J. Rademacker,[20] D. M. Asner,[21] K. W. Edwards,[21] J. Reed,[21] A. N. Robichaud,[21] and G. Tatishvili[21]

(CLEO Collaboration)

[1]*Carnegie Mellon University, Pittsburgh, Pennsylvania 15213, USA*
[2]*Enrico Fermi Institute, University of Chicago, Chicago, Illinois 60637, USA*
[3]*Cornell University, Ithaca, New York 14853, USA*
[4]*University of Florida, Gainesville, Florida 32611, USA*
[5]*George Mason University, Fairfax, Virginia 22030, USA*
[6]*University of Illinois, Urbana-Champaign, Illinois 61801, USA*
[7]*Indiana University, Bloomington, Indiana 47405, USA*
[8]*University of Kansas, Lawrence, Kansas 66045, USA*
[9]*Luther College, Decorah, Iowa 52101, USA*
[10]*University of Minnesota, Minneapolis, Minnesota 55455, USA*
[11]*Northwestern University, Evanston, Illinois 60208, USA*
[12]*University of Oxford, Oxford OX1 3RH, UK*
[13]*University of Puerto Rico, Mayaguez, Puerto Rico 00681*
[14]*Purdue University, West Lafayette, Indiana 47907, USA*
[15]*Rensselaer Polytechnic Institute, Troy, New York 12180, USA*
[16]*Rice University; Houston; Texas 77005, USA*
[17]*University of Rochester, Rochester, New York 14627, USA*
[18]*Syracuse University, Syracuse, New York 13244, USA*
[19]*Wayne State University, Detroit, Michigan 48202, USA*
[20]*University of Bristol, Bristol BS8 1TL, UK*
[21]*Carleton University, Ottawa, Ontario, Canada K1S 5B6*

We exploit the quantum coherence between pair-produced $D^0$ and $\bar{D}^0$ in $\psi(3770)$ decays to make a first determination of the relative strong phase differences between $D^0 \to K_S^0 \pi^+ \pi^-$ and $\bar{D}^0 \to K_S^0 \pi^+ \pi^-$, which are of great importance in determining the Cabibbo-Kobayashi-Maskawa angle $\gamma/\phi_3$ in $B^- \to D^0(\bar{D}^0)K^-$ decays. Using 818 pb$^{-1}$ of $e^+e^-$ collision data collected with the CLEO-c detector at $E_{cm} = 3.77$ GeV, we employ a binned Dalitz-plot analysis of $K_S^0 \pi^+ \pi^-$ and $K_L^0 \pi^+ \pi^-$ decays recoiling against flavor-tagged, $CP$-tagged, and $K_S^0 \pi^+ \pi^-$-tagged events to determine these strong phase differences.

---

*Deceased

032002-1

## I. INTRODUCTION

A central goal of flavor physics is the determination of all elements of the Cabibbo-Kobayashi-Maskawa (CKM) matrix [1], magnitudes and phases. Of the three angles of the $b - d$ CKM unitarity triangle, denoted $\alpha$, $\beta$, and $\gamma$ by some, $\phi_2$, $\phi_1$, and $\phi_3$ by others, the least-well determined is $\gamma/\phi_3$, the phase of $V_{ub}$ relative to $V_{cb}$. It is of great interest to determine $\gamma/\phi_3$ using the decay $B^{\pm} \rightarrow K^{\pm}\tilde{D}^0$, since in this mode the $\gamma/\phi_3$ value obtained is expected to be insensitive to new physics effects in $B$ decays. Thus it becomes a firm standard model reference for *CP* violation phenomena. Here, $\tilde{D}^0$ is either $D^0$ or $\bar{D}^0$, and both decay to the same final state, and so their amplitudes add. Sensitivity to the angle $\gamma/\phi_3$ comes from the interference between two Cabibbo-suppressed diagrams: $b \rightarrow c\bar{u}s$, giving rise to $B^- \rightarrow K^-D^0$, and the color and CKM-suppressed process $b \rightarrow u\bar{c}s$, giving rise to $B^- \rightarrow K^-\bar{D}^0$. One of the most promising $\tilde{D}^0$ decays for measuring $\gamma/\phi_3$ using this method is $\tilde{D}^0 \rightarrow K^0_S\pi^+\pi^-$, because it is Cabibbo favored (CF) for both $D^0$ and $\bar{D}^0$ decays, thus providing large event yields. To make use of this decay, however, the interference effects between $B^- \rightarrow K^-\bar{D}^0(\rightarrow K^0_S\pi^+\pi^-)$ and $B^- \rightarrow K^-D^0(\rightarrow K^0_S\pi^+\pi)$ need to be understood. These interference effects can be measured using CLEO-c data.

We first write the amplitude for the $B^{\pm}$ decay as follows:

$$\mathcal{A}\left(B^{\pm} \rightarrow K^{\pm}\tilde{D}^0, \tilde{D}^0 \rightarrow K^0_S\pi^+\pi^-(x, y)\right)$$
$$\propto f_D(x, y) + r_B e^{i\theta_{\pm}} f_{\bar{D}}(x, y). \qquad (1)$$

Here, $x \equiv m^2_{K^0_S\pi^+}$, $y \equiv m^2_{K^0_S\pi^-}$ are the Dalitz-plot variables in the $\tilde{D}^0$ decay, $f_D(x, y)(f_{\bar{D}}(x, y))$ is the amplitude for $D^0(\bar{D}^0)$ decay to $K^0_S\pi^+\pi^-$ at $(x, y)$, $r_B$ is the ratio of the suppressed to favored amplitudes, and $\theta_{\pm} \equiv \delta_B \pm \gamma$, where $\delta_B$ is the strong phase shift between the color-favored and color-suppressed amplitudes. Ignoring the second-order effects of charm mixing and *CP* violation [2–5], we have $f_{\bar{D}}(x, y) = f_D(y, x)$, and Eq. (1) can then be rewritten as

$$\mathcal{A}\left(B^{\pm} \rightarrow K^{\pm}\tilde{D}^0, \tilde{D}^0 \rightarrow K^0_S\pi^+\pi^-(x, y)\right)$$
$$\propto f_D(x, y) + r_B e^{i\theta_{\pm}} f_D(y, x). \qquad (2)$$

The square of the amplitude clearly depends on the phase difference $\Delta\delta_D \equiv \delta_D(x, y) - \delta_D(y, x)$, where $\delta_D(x, y)$ is the phase of $f_D(x, y)$. Thus, for the determination of $\gamma/\phi_3$, one must know $\Delta\delta_D(x, y)$. Once $\Delta\delta_D(x, y)$ is determined then a simultaneous fit to $B^+ \rightarrow D_{CP\pm}K^+$ and $B^- \rightarrow D_{CP\pm}K^-$ data allows the separate determination of $r_B$, $\delta_B$ and $\gamma$ [2].

Previous analyses, reported by the *BABAR* [6,7] and Belle [8] collaborations, extracted $\Delta\delta_D(x, y)$ by fitting a flavor-tagged $D^0 \rightarrow K^0_S\pi^+\pi^-$ Dalitz plot to a model for $D^0$ decay involving various 2-body intermediate states. Such an approach introduces a $7° \sim 9°$ model uncertainty in the value of $\gamma/\phi_3$,[1] which would be a limiting uncertainty for LHCb [9] and future *B*-factory experiments.

In the analysis presented here, we employ a model-independent approach to obtain $\Delta\delta_D(x, y)$ as suggested by Giri *et al.* [2], by exploiting the quantum coherence of $D^0 - \bar{D}^0$ pairs at the $\psi(3770)$. Because of this quantum correlation, $K^0_S\pi^+\pi^-$ and $K^0_L\pi^+\pi^-$ decays recoiling against flavor tags, *CP* tags, and $D^0 \rightarrow K^0_S\pi^+\pi^-$ tags, taken together provide direct sensitivity to the quantities $\cos\Delta\delta_D$ and $\sin\Delta\delta_D$. This measurement will result in a substantial reduction in the systematic uncertainty associated with the interference effects between $B^- \rightarrow K^-\bar{D}^0(\rightarrow K^0_S\pi^+\pi^-)$ and $B^- \rightarrow K^-D^0(\rightarrow K^0_S\pi^+\pi)$.

## II. FORMALISM

Giri *et al.* proposed [2] a model-independent procedure for obtaining $\Delta\delta_D(x, y)$, as follows. The Dalitz plot is divided into $2\mathcal{N}$ bins, symmetrically about the line $x = y$. The bin index $i$ ranges from $-\mathcal{N}$ to $+\mathcal{N}$, excluding zero. The coordinate exchange $x \leftrightarrow y$ thus corresponds to the exchange of bins $i \leftrightarrow -i$. The number of events in the $i$-th bin of a flavor-tagged $K^0_S\pi^+\pi^-$ Dalitz plot from a $D^0$ decay is then expressed as

$$K_i = A_D \int_i |f_D(x, y)|^2 dxdy = A_D F_i, \qquad (3)$$

where $A_D$ is a normalization factor. The interference between the $D^0$ and $\bar{D}^0$ amplitudes is parametrized by two quantities

$$c_i \equiv \frac{1}{\sqrt{F_i F_{-i}}} \int_i |f_D(x, y)||f_D(y, x)| \cos[\Delta\delta_D(x, y)]dxdy, \qquad (4)$$

and

$$s_i \equiv \frac{1}{\sqrt{F_i F_{-i}}} \int_i |f_D(x, y)||f_D(y, x)| \sin[\Delta\delta_D(x, y)]dxdy, \qquad (5)$$

where the integral is performed over a single bin. The parameters $c_i$ and $s_i$ are the amplitude-weighted averages of $\cos\Delta\delta_D$ and $\sin\Delta\delta_D$ over each Dalitz-plot bin. It is important to note that $c_i$ and $s_i$ depend only on the $D^0$ decay, not the $B$ decay, and therefore CLEO-c data are currently most suitable to measure these quantities. In principle they could be left as free parameters in a $\tilde{D}^0 \rightarrow K^0_S\pi^+\pi^-$ Dalitz-plot analysis from $B^{\pm}$ decays, but their values can be more precisely determined from correlated

---

[1] *BABAR* claims 5° uncertainty on $\gamma/\phi_3$ in Ref. [7] by combining $K^0_S K^+ K^-$ and $K^0_S\pi^+\pi^-$ modes.

$D^0\bar{D}^0$ pairs produced in CLEO-c. A Monte Carlo study indicates that reaching an accuracy of 2° would require an unrealistically large sample of $5 \times 10^6$ reconstructed $B^- \rightarrow \tilde{D}^0 K^-$ decays which corresponds to a 5000 ab$^{-1}$ sample at a B-factory [10].

Though the original idea of Giri et al. was to divide the Dalitz plot into square bins [2], Bondar et al. noted [10] that increased sensitivity is obtained if the bins are chosen to minimize the variation in $\Delta\delta_D$ over each bin. Thus, we divide the Dalitz phase space into $\mathcal{N}$ bins of $\Delta\delta_D$, as predicted by the BABAR isobar model [6], each of equal size in $\Delta\delta_D$. In the half of the Dalitz plot $m^2(K_S^0\pi^+) < m^2(K_S^0\pi^-)$, the i-th bin is defined by the condition

$$2\pi(i - 3/2)/\mathcal{N} < \Delta\delta_D(x, y) < 2\pi(i - 1/2)/\mathcal{N}. \quad (6)$$

The $-i$-th bin is defined symmetrically in the lower portion of the Dalitz plot. Such a binning with $\mathcal{N} = 8$ is shown in Fig. 1. One might suspect that because we are using a model to determine our bins, we are not free of model dependence. In fact any binning is correct in that it will give a correct, unbiased answer for $\gamma/\phi_3$, at the cost of larger uncertainties compared to an optimal binning with respect to $\Delta\delta_D$.

We now describe how CLEO-c data can be used to determine $c_i$ and $s_i$. The event yields in the i-th bin of both flavor-tagged and CP-tagged $\tilde{D}^0 \rightarrow K_S^0\pi^+\pi^-$ Dalitz plot are required. Because the $\psi(3770)$ has $C = -1$, the CP of the $\tilde{D}^0 \rightarrow K_S^0\pi^+\pi^-$ decay can be determined by reconstructing the companion $\tilde{D}^0$ in a CP eigenstate. With a CP-tagged $\tilde{D}^0 \rightarrow K_S^0\pi^+\pi^-$ decay, the amplitude is given by
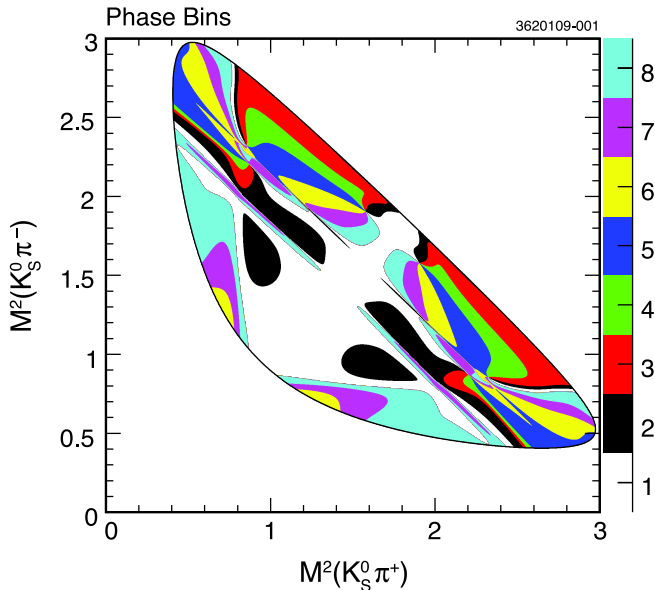


Phase Bins

FIG. 1 (color online). Phase binning of the $D^0 \rightarrow \bar{K}_S^0\pi^+\pi^-$ Dalitz plot.

$$f_{CP\pm}(x, y) = \frac{1}{\sqrt{2}}[f_D(x, y) \pm f_D(y, x)], \quad (7)$$

for CP-even and CP-odd states of a $\tilde{D}^0 \rightarrow K_S^0\pi^+\pi^-$ decay. Since the event rate is proportional to the square of this amplitude, the number of events in the i-th bin of a CP-tagged Dalitz plot is then

$$M_i^\pm = h_{CP\pm}(K_i \pm 2c_i\sqrt{K_iK_{-i}} + K_{-i}), \quad (8)$$

where $h_{CP\pm} = S^\pm/2S_f$ is a normalization factor that depends on the number $S_f$ of single flavor-tagged signal decays, and the number $S^\pm$ of single CP-tagged signal decays. Thus, access to $c_i$ is enabled by measuring the number of events $M_i^\pm$ in a CP-tagged $K_S^0\pi^+\pi^-$ Dalitz plot, and the number of events $K_i$ in a flavor-tagged $K_S^0\pi^+\pi^-$ Dalitz plot.

Unfortunately, as evident from Eq. (4), the sign of $\Delta\delta_D$ is undetermined in each of the i bins. However, sensitivity to both $c_i$ and $s_i$ can be obtained by analyzing $D^0 \rightarrow K_S^0\pi^+\pi^-$ vs $\bar{D}^0 \rightarrow K_S^0\pi^+\pi^-$ data. The amplitude for $\psi(3770)$ decays to two $K_S^0\pi^+\pi^-$ decays is as follows:

$$f(x, y, x', y') = \frac{f_D(x, y)f_D(y', x') - f_D(x', y')f_D(y, x)}{\sqrt{2}}. \quad (9)$$

The primed and unprimed Dalitz-plot coordinates correspond to the Dalitz-plot variables of the two $\tilde{D}^0 \rightarrow K_S^0\pi^+\pi^-$ decays and the minus sign is due to the $\psi(3770)$ initial state with $C = -1$. Defining $M_{ij}$ as the event rate in the i-th bin of the first and the j-th bin of the second $\tilde{D}^0 \rightarrow K_S^0\pi^+\pi^-$ Dalitz plots, respectively, we have

$$M_{ij} = h_{corr}(K_iK_{-j} + K_{-i}K_j - 2\sqrt{K_iK_{-j}K_{-i}K_j}$$
$$\times (c_ic_j + s_is_j)). \quad (10)$$

Here, $h_{corr} = N_{D\bar{D}}/2S_f^2$, where $N_{D\bar{D}}$ is the number of $D^0\bar{D}^0$ pairs, and as before $S_f$ is the number of flavor-tagged signal decays. Equation (10) then relates the product $(c_ic_j + s_is_j)$ to the measured yields of events in the flavor-tagged $\tilde{D}^0 \rightarrow K_S^0\pi^+\pi^-$ Dalitz plot ($K_{i,j}$'s) and the yields in the $D^0 \rightarrow K_S^0\pi^+\pi^-$ vs $\bar{D}^0 \rightarrow K_S^0\pi^+\pi^-$ ($M_{ij}$'s) Dalitz plots. The sensitivity to this product leads to a four-fold ambiguity: change of sign of all $c_i$ or all $s_i$. In combination with the CP-tagged analysis though, where the sign of $c_i$ is determined, this reduces to a two-fold ambiguity. One of the two solutions can be chosen based on a weak model assumption [6].

The decay $D^0 \rightarrow K_L^0\pi^+\pi^-$, due to its close relationship with $D^0 \rightarrow K_S^0\pi^+\pi^-$, can be used to further improve the $c_i$ and $s_i$ determination. Since the $K_S^0$ and $K_L^0$ mesons are of opposite CP, and we assume the convention that $A(D^0 \rightarrow K_S^0\pi^+\pi^-) = A(\bar{D}^0 \rightarrow K_S^0\pi^-\pi^+)$; it then follows that

$A(D^0 \to K_L^0 \pi^+ \pi^-) = -A(\bar{D}^0 \to K_L^0 \pi^- \pi^+)$. Then, for $K_L^0 \pi^+ \pi^-$, the Dalitz-plot rates of Eq. (8) ($CP$ vs $D^0 \to K_S^0 \pi^+ \pi^-$) and Eq. (10) ($D^0 \to K_S^0 \pi^+ \pi^-$ vs $\bar{D}^0 \to K_S^0 \pi^+ \pi^-$) become

$$M_i^{\pm} = h_{CP\pm}(K_i' \mp 2c_i'\sqrt{K_i'K_{-i}'} + K_{-i}'), \qquad (11)$$

$$M_{ij} = h_{\text{corr}}[K_i K_{-j}' + K_{-i} K_j' + 2\sqrt{K_i K_{-j}' K_{-i} K_j'}$$
$$\times (c_i c_j' + s_i s_j')], \qquad (12)$$

for $CP$ vs $D^0 \to K_L^0 \pi^+ \pi^-$ and $D^0 \to K_S^0 \pi^+ \pi^-$ vs $\bar{D}^0 \to K_L^0 \pi^+ \pi^-$, respectively, where $c_i'$, $s_i'$ are associated with $D^0 \to K_L^0 \pi^+ \pi^-$ decay.

For $D^0 \to K_L^0 \pi^+ \pi^-$ decays to benefit our determination of $c_i$ and $s_i$, we must determine the differences $\Delta c_i \equiv c_i' - c_i$, and $\Delta s_i \equiv s_i' - s_i$. In addition to the relative sign change in Eq. (11) and (12), doubly Cabibbo-suppressed decays (DCSD) of $D^0/\bar{D}^0$ also contribute with opposite signs in $D^0 \to K_S^0 \pi^+ \pi^-$ and $D^0 \to K_L^0 \pi^+ \pi^-$ decays. We can see this by inspecting the $D^0$ decay amplitude for each Dalitz plot

$$A(K_S^0 \pi^+ \pi^-) = \frac{1}{\sqrt{2}}[A(K^0 \pi^+ \pi^-) + A(\bar{K}^0 \pi^+ \pi^-)], \quad (13)$$

$$A(K_L^0 \pi^+ \pi^-) = \frac{1}{\sqrt{2}}[A(K^0 \pi^+ \pi^-) - A(\bar{K}^0 \pi^+ \pi^-)]. \quad (14)$$

The effect of this relative minus sign is to introduce a 180° phase difference for all DCSD $K^*$ resonances in the $K_L^0 \pi^+ \pi^-$ model. We can use $U$-spin symmetry to relate the amplitudes for resonances of definite $CP$ eigenvalue, e.g. $K_{S,L}^0 \rho^0(770)$. We find that these states acquire a factor of $re^{i\delta}$. To convert a $D^0 \to K_S^0 \pi^+ \pi^-$ model to the corresponding $D^0 \to K_L^0 \pi^+ \pi^-$ model, we multiply all DCSD amplitudes by $-1$ and multiply each $CP$ eigenstate amplitude by $(1 - 2re^{i\delta})$, with $r = \tan^2\theta_C$ and $\delta = 0°$ fixed for every resonance (here $\theta_C$ is the Cabibbo angle). We then determine central values for the corrections, $\Delta c_i \equiv c_i' - c_i$, $\Delta s_i \equiv s_i' - s_i$ using the $D^0 \to K_S^0 \pi^+ \pi^-$ *BABAR* model [6]. We ascribe uncertainty to both the choice of $r$ and $\delta$, as well as the usage of the *BABAR* model to determine the uncertainties on $\Delta c_i$ and $\Delta s_i$. The former are estimated by varying the phase $\delta$ between 0 and $2\pi$, and $r$ by $\pm 50\%$. For the latter, we estimate $\Delta c_i$ and $\Delta s_i$ using the Belle [8] and CLEO [11] $D^0 \to K_S^0 \pi^+ \pi^-$ isobar model fits, and take the largest resulting deviation from the value found with the *BABAR* model as a model-dependent systematic uncertainty. The total systematic uncertainties in the corrections are the quadrature sum of these two uncertainties. The central values and uncertainties on $\Delta c_i$ and $\Delta s_i$ are shown in Table I.

## III. EVENT SELECTION

We analyze 818 pb$^{-1}$ of $e^+e^-$ collision data produced by the Cornell Electron Storage Ring (CESR) at $E_{\text{cm}} = 3.77$ GeV and collected with the CLEO-c detector. The CLEO-c detector is a general purpose solenoidal detector which includes a tracking system for measuring momentum and specific ionization ($dE/dx$) of charged particles, a ring imaging Cherenkov detector (RICH) to aid in particle identification, and a CsI calorimeter for detection of electromagnetic showers. The CLEO-c detector is described in detail elsewhere [12].

Standard CLEO-c selection criteria for $\pi^{\pm}$, $K^{\pm}$, $\pi^0$, and $K_S^0$ candidates are used, and are described in Ref. [13]. To distinguish electrons from hadrons, we use a multivariate discriminant [14] that combines information from the ratio of the energy deposited in the calorimeter to the measured track momentum ($E/p$), ionization energy loss in the tracking chamber ($dE/dx$), and the ring-imaging Cherenkov counter. For $K_S^0$ decays, we select candidates with $|M(\pi^+\pi^-) - M_{K_S^0}| < 7.5$ MeV/$c^2$, and require the decay vertex to be separated from the interaction region with a significance greater than 2 standard deviations (except for $D^0 \to K_S^0 \pi^+ \pi^-$ vs $\bar{D}^0 \to K_S^0 \pi^+ \pi^-$ candidates). Reconstruction of $\eta \to \gamma\gamma$ proceeds analogously to $\pi^0 \to \gamma\gamma$, with the requirement that $|M(\gamma\gamma) - M_\eta| < 42$ MeV/$c^2$. We form $\omega \to \pi^+\pi^-\pi^0$ candidates and re-

TABLE I.  Predicted values for $\Delta c_i \equiv c_i' - c_i$ and $\Delta s_i \equiv s_i' - s_i$ with the systematic uncertainties.

| $i$ | $c_i$ | $c_i'$ | $\Delta c_i$ | $s_i$ | $s_i'$ | $\Delta s_i$ |
|---|---|---|---|---|---|---|
| 1 | 0.769 | 0.868 | $0.099 \pm 0.040$ | 0.032 | $-0.002$ | $-0.034 \pm 0.068$ |
| 2 | 0.570 | 0.737 | $0.167 \pm 0.029$ | 0.396 | 0.332 | $-0.064 \pm 0.084$ |
| 3 | $-0.044$ | 0.283 | $0.327 \pm 0.122$ | 0.765 | 0.752 | $-0.013 \pm 0.097$ |
| 4 | $-0.570$ | $-0.317$ | $0.253 \pm 0.192$ | 0.644 | 0.777 | $0.133 \pm 0.136$ |
| 5 | $-0.842$ | $-0.765$ | $0.077 \pm 0.061$ | $-0.152$ | $-0.111$ | $0.041 \pm 0.080$ |
| 6 | $-0.626$ | $-0.406$ | $0.220 \pm 0.084$ | $-0.574$ | $-0.612$ | $-0.038 \pm 0.065$ |
| 7 | $-0.006$ | 0.410 | $0.416 \pm 0.160$ | $-0.766$ | $-0.671$ | $0.095 \pm 0.063$ |
| 8 | 0.410 | 0.594 | $0.184 \pm 0.024$ | $-0.386$ | $-0.371$ | $0.015 \pm 0.086$ |

TABLE II. Single-tag and $K_{S/L}^0 \pi^+ \pi^-$ double-tag yields.

| Mode | ST yield | $K_S^0 \pi^+ \pi^-$ yield | $K_L^0 \pi^+ \pi^-$ yield |
|---|---|---|---|
| Flavor tags | | | |
| $K^- \pi^+$ | $144\,563 \pm 403$ | 1447 | 2858 |
| $K^- \pi^+ \pi^0$ | $258\,938 \pm 581$ | 2776 | 5130 |
| $K^- \pi^+ \pi^+ \pi^-$ | $220\,831 \pm 541$ | 2250 | 4110 |
| $K^- e^+ \nu$ | $123\,412 \pm 4591$ | 1356 | |
| | | | |
| $CP$-even tags | | | |
| $K^+ K^-$ | $12\,867 \pm 126$ | 124 | 345 |
| $\pi^+ \pi^-$ | $5950 \pm 112$ | 62 | 172 |
| $K_S^0 \pi^0 \pi^0$ | $6562 \pm 131$ | 56 | |
| $K_L^0 \pi^0$ | $27\,955 \pm 2013$ | 229 | |
| | | | |
| $CP$-odd tags | | | |
| $K_S^0 \pi^0$ | $19\,059 \pm 150$ | 189 | 281 |
| $K_S^0 \eta$ | $2793 \pm 69$ | 39 | 41 |
| $K_S^0 \omega$ | $8512 \pm 107$ | 83 | |
| $K_S^0 \pi^+ \pi^-$ tags | | 475 | 867 |

quire their mass to be within 20 MeV of the nominal $\omega$ mass [15].

In this analysis, we reconstruct $D^0$ mesons in several flavor-tagged modes, $CP$-tagged modes, and in $K_S^0 \pi^+ \pi^-$. From these selected events, we also reconstruct the companion $D^0$ from the $\psi(3770)$ decay in either $K_S^0 \pi^+ \pi^-$ or $K_L^0 \pi^+ \pi^-$ to form "double tags." The single-tag yields enter our analysis through the $S_f$ and $S^\pm$ factors, whereas the double tags provide the $K_i$, $M_i$, and $M_{ij}$ yields across their respective Dalitz plots. The double-tagged events we consider are shown in Table II (all the notations include charge conjugate if not otherwise specified). We thus consider flavor tags: $K^- \pi^+$, $K^- \pi^+ \pi^0$, $K^- \pi^+ \pi^+ \pi^-$; semi-leptonic tag: $K^- e^+ \nu$; $CP$-even tags: $K^+ K^-$, $\pi^+ \pi^-$, $K_S^0 \pi^0 \pi^0$, $K_L^0 \pi^0$; and $CP$-odd tags: $K_S^0 \pi^0$, $K_S^0 \eta$, $K_S^0 \omega$, with $\pi^0/\eta \to \gamma\gamma$, $\omega \to \pi^+ \pi^- \pi^0$, and $K_S^0 \to \pi^+ \pi^-$. We also reconstruct double-tag (DT) events with $\tilde{D}^0 \to K_{S,L}^0 \pi^+ \pi^-$ vs $\tilde{D}^0 \to K_S^0 \pi^+ \pi^-$ as discussed in the preceding section. We do not reconstruct $K_L^0 \pi^+ \pi^-$ in some DT modes when there are two missing particles ($K^- e^+ \nu$ and $K_L^0 \pi^0$ cases) or the backgrounds are large (as for $K_S^0 \pi^0 \pi^0$ and $K_S^0 \omega$).

The event yield in the $i$-th Dalitz-plot bin of each tagged $\tilde{D}^0 \to K_{S,L}^0 \pi^+ \pi^-$ sample is determined by evaluating the phase difference for each data point according to the *BABAR* isobar model. The contribution of each isobar to the total amplitude is evaluated as a function of all three invariant mass-squared combinations computed directly from the four-momentum of the $\tilde{D}$ daughters as described in Ref. [16]. The phase difference is well defined beyond and continues smoothly across the kinematically allowed Dalitz-plot boundary. A small number of candidate events ($\sim 1$–3% depending on tag and signal mode) included in this analysis are reconstructed outside the kinematically allowed region due to finite detector resolution.

## A. Single tags

The $\psi(3770)$ resonance is below threshold for $D\bar{D}\pi$ production, and so the events of interest $e^+ e^- \to \psi(3770) \to D\bar{D}$ have $D$ mesons with energy equal to the beam energy and a unique momentum. Thus, for identifying $D^0$ candidates, we follow Mark III [17] and define two kinematic variables: the beam-constrained candidate mass $M_{\text{bc}} \equiv \sqrt{E_0^2/c^4 - \mathbf{P}_D^2/c^2}$, where $\mathbf{P}_D$ is the $D^0$ candidate momentum and $E_0$ is the beam energy; and $\Delta E \equiv E_D - E_0$, where $E_D$ is the sum of the $D^0$ candidate daughter energies. Candidate tags are required to have $\Delta E$ within about 3 standard deviations of zero [18].

For events with a $K^- \pi^+$, $K^+ K^-$, and $\pi^+ \pi^-$ single tag (ST) that have no additional charged particles, we apply additional selection requirements to suppress cosmic ray muons and Bhabha events. We do not allow tracks identified as electrons or muons to be used in the tag. We demand evidence of the other $D$ by requiring at least one electromagnetic shower in the calorimeter above 50 MeV not associated with the tracks of the tag, where a single minimum ionizing particle deposits the equivalent of 200 MeV. For $K^+ K^-$ ST candidates, additional geometric requirements are needed to remove doubly radiative Bhabha events followed by pair conversion of a radiated photon. We accept only one candidate per mode per event; when multiple candidates are present, we choose the one with smallest $|\Delta E|$.

The resulting $M_{\text{bc}}$ distributions are shown in Fig. 2. Each distribution is fit to a signal shape derived from simulated signal events and to a background ARGUS [19] threshold function. The ST yield is given by the area in the signal peak in the mass region from $1.86 < M_{\text{bc}} < 1.87$ GeV.

## B. Double tags with $K_S^0 \pi^+ \pi^-$

We form $K_S^0 \pi^+ \pi^-$ DTs by combining a $K_S^0 \pi^+ \pi^-$ tag with a ST candidate. We choose one DT candidate per mode per event with $\bar{M}$ closest to the measured $D^0$ mass, where $\bar{M} \equiv [M(D^0) + M(\bar{D}^0)]/2$.

Since the $D^0 \to K_S^0 \pi^+ \pi^-$ vs $\bar{D}^0 \to K_S^0 \pi^+ \pi^-$ sample plays a key role in extracting $s_i$ values, we drop the requirement on the flight distance significance for $K_S^0$ candidates to increase the statistics. We find 421 $D^0 \to K_S^0 \pi^+ \pi^-$ vs $\bar{D}^0 \to K_S^0 \pi^+ \pi^-$ candidates which include about 9% background. We increase the yield by about 15% (additional 54 candidates, $\sim$15% background) by reconstructing the $K_S^0 \pi^+ \pi^-$ vs $K_S^0 \pi^+ \pi^-$ candidates when one $\pi^\pm$ is not reconstructed. The presence of the $\pi^\pm$ is inferred from the missing four-momentum calculated from the well known initial state and the reconstructed particles.

## C. Double tags with $K^- e^+ \nu$

Candidate $K^- e^+ \nu$ vs $K_S^0 \pi^+ \pi^-$ DTs are reconstructed by combining a $K_S^0 \pi^+ \pi^-$ ST candidate with a kaon candidate and an electron candidate from the remainder of the
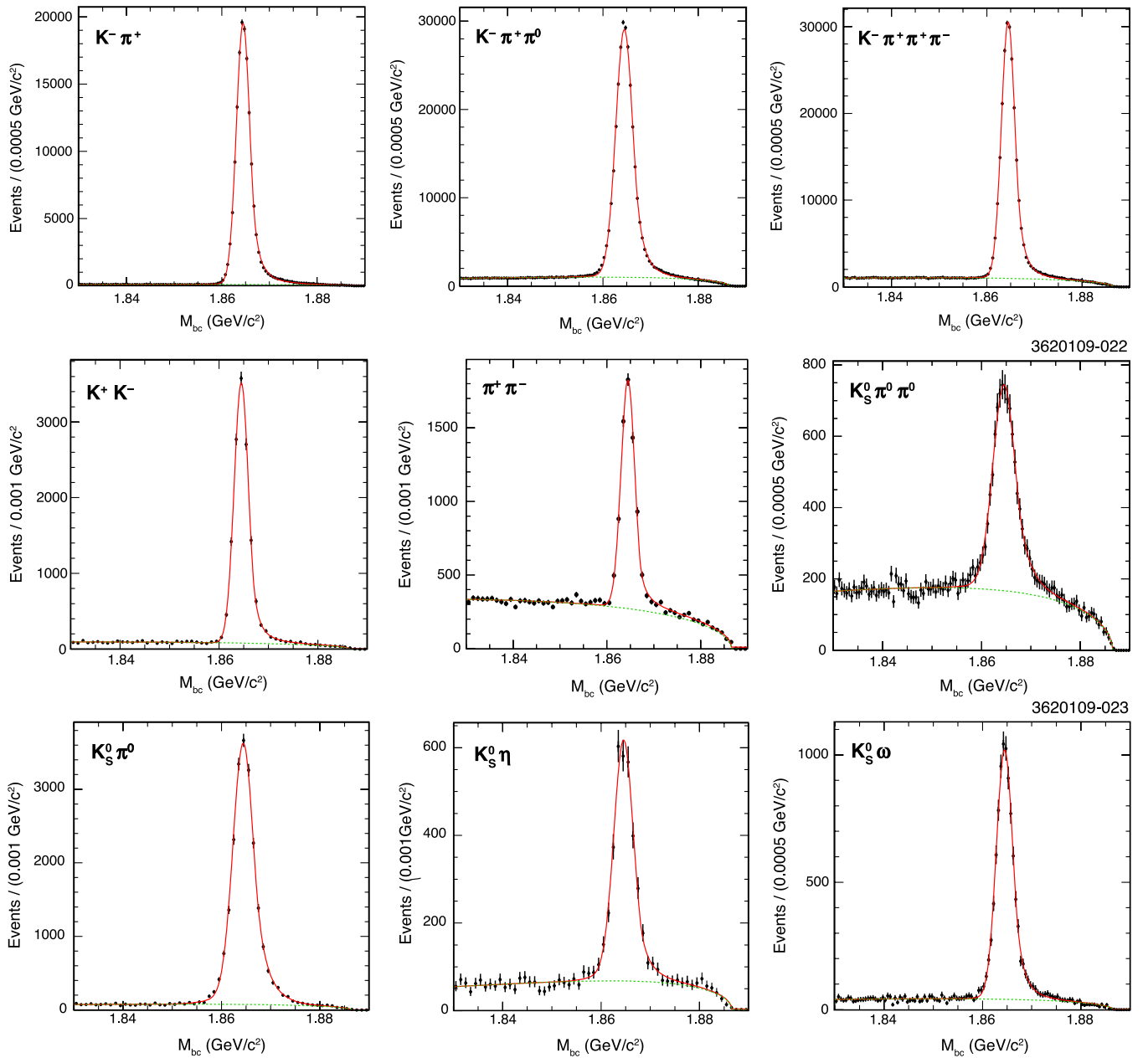
FIG. 2 (color online).   Data $M_{bc}$ distribution for various tag modes. The solid lines show the total fits, and the dashed lines show the background shapes.

event. Events with more than two additional tracks (aside from the $K_S^0 \pi^+ \pi^-$ daughters) are vetoed. Signal discrimination for $D \to K^- e^+ \nu$ uses the variable $U \equiv E_{miss} - c|\vec{\mathbf{p}}_{miss}|$, where $E_{miss}$ and $\vec{\mathbf{p}}_{miss}$ are the missing energy and momentum in the semileptonic $D^0$ meson decay, calculated using the difference of the four-momenta of the tag and that of the $K^-$ and $e^+$ candidates. For correctly identified events, $U = 0$, since only the neutrino is undetected. After all selection criteria are applied, multiple candidates are rare for $K^- e^+ \nu$. The $U$ distribution for $D^0 \to K^- e^+ \nu$ candidates is shown in Fig. 3. The points with error bars are

data and the shaded histogram represents a simulation of the background, which is less than 1% in the signal region, $|U| < 50$ MeV.

### D. Double tags with $K_L^0 \pi^0$

The $K_S^0 \pi^+ \pi^-$ vs $K_L^0 \pi^0$ DT mode is reconstructed with a missing-mass technique since the $K_L^0$ mesons produced at CLEO-c are not reconstructed. A fully reconstructed $K_S^0 \pi^+ \pi^-$ ST is combined with a $\pi^0$ candidate, and we compute the recoil-mass squared against the ST-$\pi^0$ system $M^2_{miss}$. Signal $K_L^0 \pi^0$ decays are identified by a peak in $M^2_{miss}$
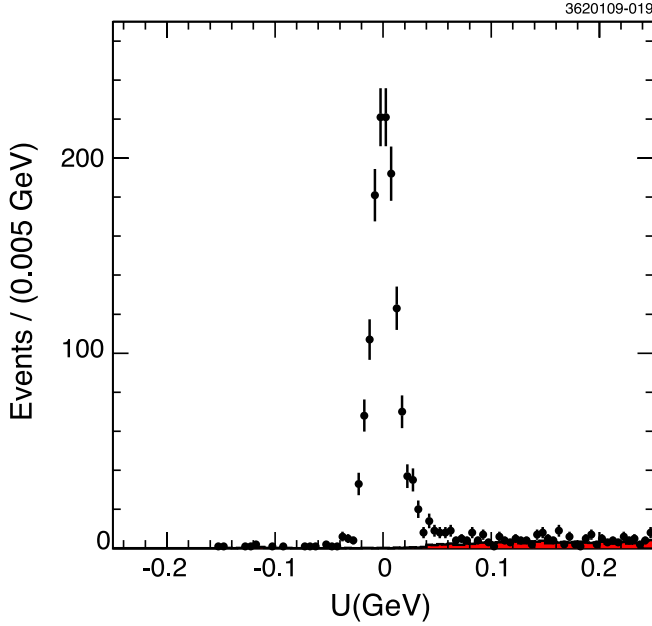
FIG. 3 (color online). $U \equiv E_{\mathrm{miss}} - c|\vec{\mathbf{p}}_{\mathrm{miss}}|$ distribution for $K^- e^+ \nu$ in events with a $D^0 \to K_S^0 \pi^+ \pi^-$ signal candidate. The points with error bars are data and the shaded histogram represents a simulation of the backgrounds.

at $M_{K_L^0}^2$. Backgrounds from $D \to K_S^0 \pi^0$, $\pi^0 \pi^0$, and $\eta \pi^0$ are suppressed by vetoing events with additional unassigned charged particles, or $\eta \to \gamma\gamma$ or $\pi^0 \to \gamma\gamma$ candidates. We further suppress backgrounds by making requirements on the energy of showers in the calorimeter that are not associated with the decay products of the $K_S^0 \pi^+ \pi^-$ or the $\pi^0$. We compute the angle $\theta$ between each unassigned shower and the direction of the missing momentum. For $\cos\theta < 0.9$, we require the energy of showers $E_{\mathrm{shower}} <$ 100 MeV for any single shower. If $0.9 < \cos\theta < 0.98$, we require $E_{\mathrm{shower}} < 100 + 250 \times (\cos\theta - 0.9)$ MeV. The $M_{\mathrm{miss}}^2$ distribution for $K_L^0 \pi^0$ is shown in Fig. 4. The points with error bars are data and the shaded histogram represents a simulation of the backgrounds. Signal candidates are required to be within the range $0.1 < M_{\mathrm{miss}}^2 < 0.5$ GeV$^2/c^4$.

## E. Double tags with $K_L^0 \pi^+ \pi^-$

Candidate $K_L^0 \pi^+ \pi^-$ decays are reconstructed in DTs using a similar missing-mass technique as described in Sec. III D. We require the signal side (associated with the $K_L^0 \pi^+ \pi^-$ candidate) to have exactly two charged tracks. Backgrounds are reduced by applying $\pi^0$, $\eta$, and $K_S^0$ vetoes. Using the measured momenta of the tagged $D^0$ and the two additional pions, we compute the missing momentum and missing energy on the signal side. We apply the same requirements to the energy of the unassigned showers as described in Sec. III D. The $M_{\mathrm{miss}}^2$ dis-
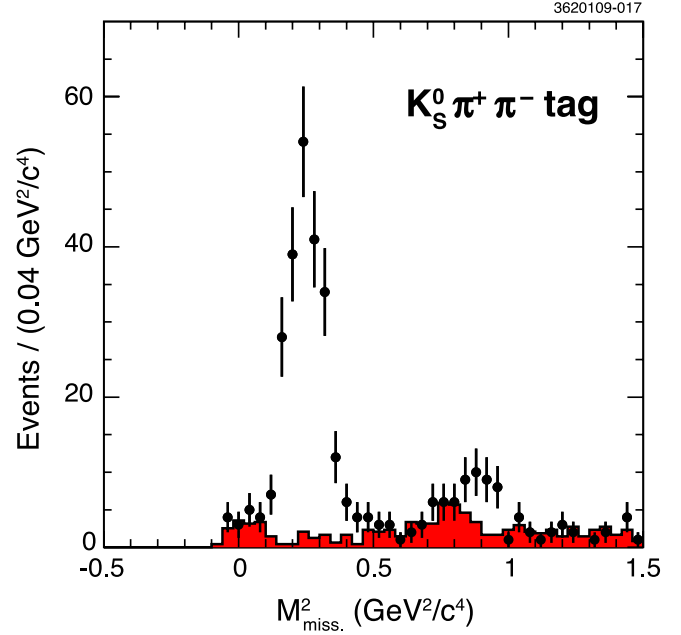


FIG. 4 (color online). $M_{\mathrm{miss}}^2$ distributions for $K_L^0 \pi^0$ when one $D$ is identified as $K_S^0 \pi^+ \pi^-$. The points with error bars are data, and the shaded histogram represents the simulation of the backgrounds. The enhancement of the data relative to the simulated backgrounds near 0.9 GeV$^2/c^4$ corresponds to the decay $K^{*0} \pi^0 \to K_L^0 \pi^0 \pi^0$ where both the $K_L^0$ and $\pi^0$ from the $K^{*0}$ are undetected. The Dalitz-plot model of this process is not implemented in our simulation.

tributions for $K_L^0 \pi^+ \pi^-$ are shown in Fig. 5. The points with error bars are data and the shaded histograms show a simulation of the backgrounds. Signal events are required to have a missing-mass squared in the region $0.21 < M_{\mathrm{miss}}^2 < 0.29$ GeV$^2/c^4$.

## F. Yields in data

The ST yields for the tag modes and DT yields for $K_{S/L}^0 \pi^+ \pi^-$ versus different tags are shown in Table II. To determine the $D^0 \to K^- e^+ \nu$ and $D^0 \to K_L^0 \pi^0$ ST yields we use the integrated luminosity, measured $D^0 \bar{D}^0$ cross sections [13], and measured branching fractions [20,21]. Combining all modes of the same $CP$, we show in Fig. 6 the Dalitz-plot distribution of $CP$-even and $CP$-odd tagged $\tilde{D}^0 \to K_S^0 \pi^+ \pi^-$ decays. Figure 7 shows the corresponding distributions for $CP$-tagged $\tilde{D}^0 \to K_L^0 \pi^+ \pi^-$ decays. The clear absence of a $\rho^0 K_S^0$ component ($CP$-odd) in $CP$-odd tagged $K_S^0 \pi^+ \pi^-$ decays is an illustration of the quantum correlations that exist in the $\psi(3770) \to D^0 \bar{D}^0$ decay. For $K_L^0 \pi^+ \pi^-$, $\rho^0 K_L^0$ is absent in the $CP$-even tagged samples.

The signal-to-background ratios in our $K_{S/L}^0 \pi^+ \pi^-$ DT samples range from 10 to better than 100, depending on tag mode. The tag side $\Delta E$, $K_S^0$, and $\omega$ sidebands are used for combinatorial and nonresonant background subtraction.
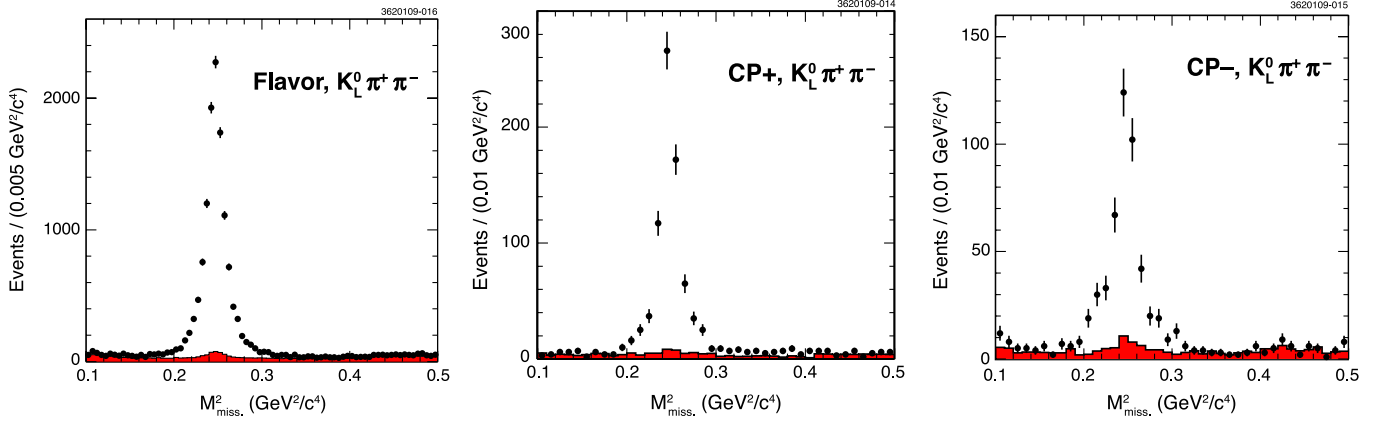
FIG. 5 (color online).   $M^2_{\mathrm{miss}}$ distributions for $K^0_L\pi^+\pi^-$ for flavor tags (left), *CP*-even tags (middle), and *CP*-odd tags (right). The points with error bars are data and the shaded histograms represent simulations of the backgrounds.
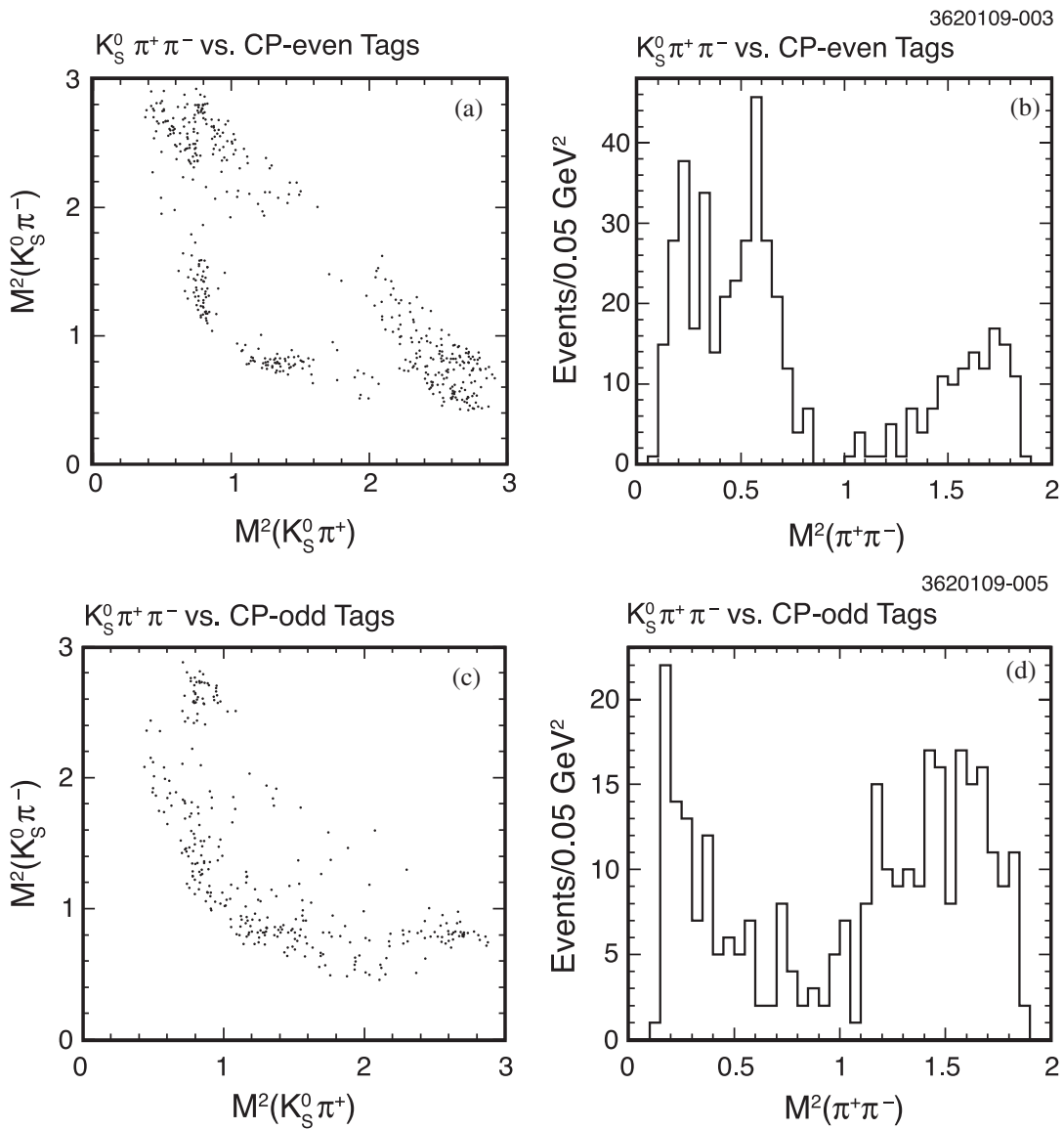


FIG. 6.   *CP*-even tagged $K^0_S\pi^+\pi^-$ Dalitz plot (a), and its $m^2(\pi^+\pi^-)$ projection (b). *CP*-odd tagged $K^0_S\pi^+\pi^-$ Dalitz plot (c), and its $m^2(\pi^+\pi^-)$ projection (d).

FIG. 7.   *CP*-even tagged $K_L^0 \pi^+ \pi^-$ Dalitz plot (a), and its $m^2(\pi^+ \pi^-)$ projection (b). *CP*-odd tagged $K_L^0 \pi^+ \pi^-$ Dalitz plot (c), and its $m^2(\pi^+ \pi^-)$ projection (d).
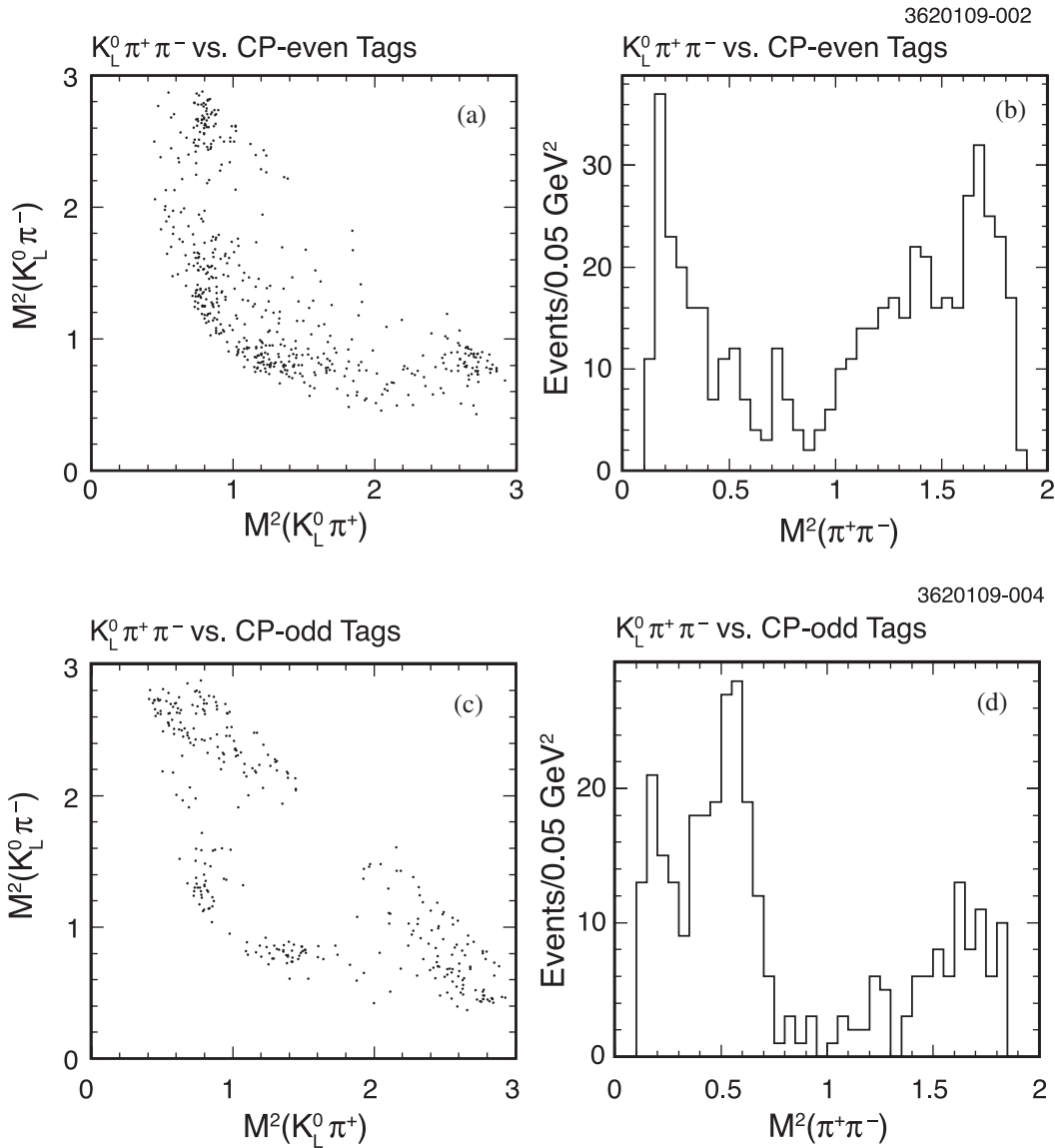
On the signal side, the background level is 1.9% for $K_S^0 \pi^+ \pi^-$ after applying the $K_S^0$ flight significance requirement. This part of the background is considered as a systematic error. The background-to-signal ratio for the $K_L^0 \pi^+ \pi^-$ signal side is about 5%, of which about 2% is a peaking background from $K_S^0 \pi^+ \pi^-$, $K_S^0 \to \pi^0 \pi^0$ decays that pass the $K_L^0 \pi^+ \pi^-$ selection criteria. We estimate this peaking background yield using $K_S^0 \pi^+ \pi^-$ data and a misidentification rate determined from a quantum-correlated Monte Carlo simulation. The combinatorial background contribution is estimated using the $M_{\mathrm{miss}}^2$ sidebands. The expected yields from these two background sources are subtracted from the observed signal yields to obtain background-corrected yields.

For the $K_S^0 \pi^+ \pi^-$ vs $K_S^0 \pi^+ \pi^-$ sample, no $K_S^0$ flight significance requirement was applied, resulting in a background-to-signal ratio of ~9%. About 7% (of 9%) of this background comes from $\tilde{D}^0 \to \pi^+ \pi^- \pi^+ \pi^-$ faking $K_S^0 \pi^+ \pi^-$. This background is subtracted using a Monte Carlo simulation of this decay, where the $\pi^+ \pi^- \pi^+ \pi^-$ Dalitz-plot structure is taken from the FOCUS experiment [22]. The impact of the remaining ~1.9% of background on our nominal fit results is small and included in the systematic uncertainties.

The reconstruction efficiency is defined as the ratio of reconstructed events to generated events in each bin. The reconstruction efficiencies are calculated from large Monte Carlo samples generated according to the *BABAR* model [6] following the amplitude description of Eqs. (7) and (9) for different tag modes. Dividing the observed yields in each $\delta_D$ bin by this efficiency, we obtain the efficiency-corrected yields $M_i^\pm$ and $M_{ij}$.

TABLE III. Fit results for $c_i$, $s_i$ (with $\Delta c_i$ and $\Delta s_i$ fixed), $c_i$, $c'_i$, $s_i$, and $s'_i$ (with $\Delta c_i$ and $\Delta s_i$ constrained). See Table I for $\Delta c_i$ and $\Delta s_i$.

| | $\Delta c_i$, $\Delta s_i$ fixed | | $\Delta c_i$, $\Delta s_i$ constrained | | | |
| --- | --- | --- | --- | --- | --- | --- |
| $i$ | $c_i$ | $s_i$ | $c_i$ | $c'_i$ | $s_i$ | $s'_i$ |
| 1 | $0.742 \pm 0.037$ | $0.004 \pm 0.160$ | $0.743 \pm 0.041$ | $0.840 \pm 0.041$ | $0.014 \pm 0.166$ | $-0.021 \pm 0.164$ |
| 2 | $0.606 \pm 0.071$ | $0.014 \pm 0.215$ | $0.611 \pm 0.072$ | $0.779 \pm 0.072$ | $0.014 \pm 0.216$ | $-0.069 \pm 0.219$ |
| 3 | $-0.008 \pm 0.063$ | $0.581 \pm 0.190$ | $0.059 \pm 0.077$ | $0.250 \pm 0.078$ | $0.609 \pm 0.188$ | $0.587 \pm 0.188$ |
| 4 | $-0.529 \pm 0.101$ | $0.138 \pm 0.217$ | $-0.495 \pm 0.114$ | $-0.349 \pm 0.135$ | $0.151 \pm 0.225$ | $0.275 \pm 0.232$ |
| 5 | $-0.889 \pm 0.049$ | $-0.053 \pm 0.183$ | $-0.911 \pm 0.053$ | $-0.793 \pm 0.057$ | $-0.050 \pm 0.189$ | $-0.016 \pm 0.192$ |
| 6 | $-0.742 \pm 0.066$ | $-0.317 \pm 0.187$ | $-0.736 \pm 0.070$ | $-0.546 \pm 0.080$ | $-0.340 \pm 0.194$ | $-0.388 \pm 0.200$ |
| 7 | $0.108 \pm 0.074$ | $-0.836 \pm 0.185$ | $0.157 \pm 0.092$ | $0.475 \pm 0.094$ | $-0.827 \pm 0.190$ | $-0.725 \pm 0.196$ |
| 8 | $0.403 \pm 0.046$ | $-0.410 \pm 0.158$ | $0.403 \pm 0.046$ | $0.591 \pm 0.048$ | $-0.409 \pm 0.158$ | $-0.374 \pm 0.169$ |

## IV. EXTRACTION OF $c_i$ AND $s_i$

We determine the coefficients $c_i$, $s_i$ by minimizing the negative log-likelihood function

$$-2\log\mathcal{L} = -2\sum_i \log P(M_i^{\pm}, \langle M_i^{\pm}\rangle)_{(CP, K_S^0\pi^+\pi^-)}$$
$$- 2\sum_i \log P(M_i^{\pm}, \langle M_i^{\pm}\rangle)_{(CP, K_L^0\pi^+\pi^-)}$$
$$- 2\sum_{i,j} \log P(M_{ij}, \langle M_{ij}\rangle)_{(K_S^0\pi^+\pi^-, K_S^0\pi^+\pi^-)}$$
$$- 2\sum_{i,j} \log P(M_{ij}, \langle M_{ij}\rangle)_{(K_S^0\pi^+\pi^-, K_L^0\pi^+\pi^-)} + \chi^2,$$

(15)

where $\langle M_i^{\pm}\rangle$ is calculated according Eqs. (8) and (11), and $\langle M_{ij}\rangle$ is calculated according Eqs. (10) and (12), and $P(M, \langle M\rangle)$ is the Poisson probability to get $M$ events given the expected number $\langle M\rangle$. In our nominal fit, a $\chi^2$ penalty term

$$\chi^2 = \sum_i \left(\frac{c'_i - c_i - \Delta c_i}{\delta\Delta c_i}\right)^2 + \sum_i \left(\frac{s'_i - s_i - \Delta s_i}{\delta\Delta s_i}\right)^2 \quad (16)$$

constrains $c'_i$ and $s'_i$ to differ from $c_i$ and $s_i$, respectively, by their expected differences $\Delta c_i$, $\Delta s_i$, within errors. (Those errors, $\delta\Delta c_i$, $\delta\Delta s_i$, are the systematic uncertainties shown in Table I.) This constraint has little impact on $c_i$ but is important for $s_i$ and will be relaxed and tightened as a systematic variation.

From Monte Carlo studies, we found that DCSD decays in flavor tag modes ($K^-\pi^+$, $K^-\pi^+\pi^0$, $K^-\pi^+\pi^+\pi^-$) lead to a significant bias in the $K_i^{(\prime)}$'s due to an interference of the wrong flavor of the $\tilde{D}^0 \to K_{S/L}^0\pi^+\pi^-$ decay; this results in a significant bias in the values of $c_i^{(\prime)}$ and $s_i^{(\prime)}$ from the $D^0 \to K_S^0\pi^+\pi^-$ vs $D^0 \to K_{S/L}^0\pi^+\pi^-$ analyses. Therefore, for the $D^0 \to K_L^0\pi^+\pi^-$ vs $D^0 \to K_S^0\pi^+\pi^-$ analysis, we use only the $D^0 \to K^-e^+\nu$ tagged $K_S^0\pi^+\pi^-$

sample and the $D^0 \to K^-\pi^+$ tagged $K_L^0\pi^+\pi^-$ sample for counting $S_f^{(\prime)}$ and $K_i^{(\prime)}$ yields.[2] For the latter, we estimate the biases and adjust the $K_i^{(\prime)}$ values using the correction factor

$$|A_{D^0\to K_S^0\pi^+\pi^-}|^2 / |A_{D^0\to K_S^0\pi^+\pi^-} + \mathrm{re}^{-i\delta_{K\pi}}A_{\bar{D}^0\to K_S^0\pi^+\pi^-}|^2.$$

(17)

Here $r = |A(D^0 \to K^+\pi^-)/A(D^0 \to K^-\pi^+)|$ and $\delta_{K\pi}$ are the ratio of amplitudes of the DCSD to CF decay and the relative strong phase, respectively. The amplitude ratio squared, $r^2 = (3.44 \pm 0.01 \pm 0.09) \times 10^{-3}$ and $\delta_{K\pi} = (22 \pm 16.3)°$ are taken from Ref. [18]. This correction factor is estimated in each of our eight Dalitz-plot bins using the *BABAR* $D^0 \to K_S^0\pi^+\pi^-$ Dalitz-plot fit amplitude [6]. The model dependence of this correction is negligible. Uncertainties on these corrections due to the uncertainty on $\delta_{K\pi}$ are small and are included in our systematic uncertainties.

The fitting procedure was tested using a simulated $C$-odd $D^0\bar{D}^0$ Monte Carlo sample where we performed 100 toy $K_S^0\pi^+\pi^-$ vs $K_S^0\pi^+\pi^-$ experiments with $c_i$ and $s_i$ taken from the *BABAR* model. The means and widths of the pull distributions of the $c_i$ and $s_i$ parameters were consistent with zero and one, respectively, indicating no bias and proper estimation of statistical uncertainties.

To enable the separation of the statistical uncertainty on $c_i$ and $s_i$ from the systematic uncertainty on $\Delta c_i$ and $\Delta s_i$ we perform a likelihood fit to $(c_i, s_i)$ with the values of $(c'_i, s'_i)$ fixed according to Table I. The results of this fit and of the nominal likelihood fit to $(c_i, s_i)$, $(c'_i, s'_i)$ are shown in Table III. The (statistical) correlation matrix among $c_i$ and $s_i$ in the constrained fit is shown in Table IV. Note that in Table III, we choose the $s_i$ and $s'_i$ signs based on *BABAR* isobar model predictions [6] to resolve the two-fold ambiguity discussed in Sec. II.

---

[2] All three hadronic flavor tag modes are used to determine $K_i^{(\prime)}$ for the $CP$-tag vs $K_{S/L}^0\pi^+\pi^-$ determination of $c_i^{(\prime)}$.

TABLE IV.　Correlation Matrix for the $c_i$ and $s_i$ parameters. Labels 1–8 represent $c_1$–$c_8$ and 9–16 represent $s_1$–$s_8$.

| $i$ | 1 | 2 | 3 | 4 | 5 | 6 | 7 | 8 | 9 | 10 | 11 | 12 | 13 | 14 | 15 | 16 |
|---|---|---|---|---|---|---|---|---|---|---|---|---|---|---|---|---|
| 1 | 1.000 | | | | | | | | | | | | | | | |
| 2 | −0.028 | 1.000 | | | | | | | | | | | | | | |
| 3 | −0.007 | −0.011 | 1.000 | | | | | | | | | | | | | |
| 4 | 0.035 | 0.011 | 0.002 | 1.000 | | | | | | | | | | | | |
| 5 | 0.073 | −0.022 | 0.006 | 0.004 | 1.000 | | | | | | | | | | | |
| 6 | 0.016 | 0.069 | −0.003 | 0.003 | −0.104 | 1.000 | | | | | | | | | | |
| 7 | 0.018 | 0.013 | −0.020 | 0.005 | 0.033 | 0.016 | 1.000 | | | | | | | | | |
| 8 | −0.020 | −0.028 | 0.008 | 0.005 | 0.050 | 0.013 | 0.015 | 1.000 | | | | | | | | |
| 9 | 0.024 | 0.006 | −0.072 | −0.006 | 0.014 | 0.014 | 0.113 | 0.040 | 1.000 | | | | | | | |
| 10 | 0.000 | −0.033 | 0.017 | −0.007 | −0.003 | 0.038 | −0.001 | −0.001 | −0.060 | 1.000 | | | | | | |
| 11 | 0.006 | 0.007 | −0.025 | −0.002 | 0.003 | −0.008 | 0.041 | 0.029 | 0.323 | −0.154 | 1.000 | | | | | |
| 12 | 0.004 | 0.005 | −0.020 | 0.035 | 0.002 | 0.000 | 0.014 | 0.005 | 0.149 | −0.124 | 0.244 | 1.000 | | | | |
| 13 | 0.001 | −0.001 | −0.003 | −0.014 | −0.008 | −0.072 | −0.007 | −0.004 | 0.158 | −0.107 | 0.340 | 0.070 | 1.000 | | | |
| 14 | −0.011 | −0.014 | 0.078 | 0.005 | −0.004 | −0.042 | −0.086 | −0.021 | −0.448 | 0.085 | −0.213 | −0.124 | −0.275 | 1.000 | | |
| 15 | 0.009 | 0.008 | −0.053 | −0.003 | 0.004 | 0.002 | 0.061 | 0.013 | 0.373 | −0.139 | 0.314 | 0.228 | 0.269 | −0.405 | 1.000 | |
| 16 | 0.004 | 0.004 | −0.056 | −0.004 | 0.003 | −0.007 | 0.026 | 0.041 | 0.234 | −0.096 | 0.521 | 0.176 | 0.243 | −0.133 | 0.106 | 1.000 |

## V. SYSTEMATIC UNCERTAINTIES

Systematic uncertainties on $(c_i, s_i)$ and $(c'_i, s'_i)$ come from many sources. Tables V and VI summarize the main contributions of the systematic uncertainties for $c_i$ and $s_i$, respectively. Tables VII and VIII summarize the main contributions of the systematic uncertainties for $c'_i$ and $s'_i$, respectively.

In the global fit, the fitter does not take the statistical uncertainties associated with flavor-tagged samples into account. That is $K_i^{(')}$ do not float in the global fit. We

TABLE V.　Systematic uncertainties for $c_i$.

| | $c_1$ | $c_2$ | $c_3$ | $c_4$ | $c_5$ | $c_6$ | $c_7$ | $c_8$ |
|---|---|---|---|---|---|---|---|---|
| $K_i^{(')}$ statistics error | 0.010 | 0.015 | 0.016 | 0.019 | 0.009 | 0.015 | 0.018 | 0.008 |
| Momentum resolution | 0.008 | 0.015 | 0.012 | 0.019 | 0.011 | 0.012 | 0.017 | 0.009 |
| Efficiency variation | 0.004 | 0.007 | 0.011 | 0.008 | 0.005 | 0.008 | 0.010 | 0.006 |
| Single-tag yields | 0.006 | 0.007 | 0.013 | 0.011 | 0.005 | 0.008 | 0.015 | 0.008 |
| Tag side background | 0.007 | 0.007 | 0.014 | 0.013 | 0.006 | 0.008 | 0.014 | 0.011 |
| $K_S^0 \pi^+ \pi^-$ background | 0.001 | 0.002 | 0.009 | 0.027 | 0.012 | 0.006 | 0.003 | 0.002 |
| $K_L^0 \pi^+ \pi^-$ background | 0.006 | 0.018 | 0.004 | 0.024 | 0.017 | 0.012 | 0.020 | 0.006 |
| Multi-candidate selection | 0.002 | 0.003 | 0.003 | 0.008 | 0.004 | 0.006 | 0.003 | 0.002 |
| Non-$D/\bar{D}$ | 0.010 | 0.016 | 0.004 | 0.007 | 0.004 | 0.005 | 0.006 | 0.005 |
| DCSD | 0.009 | 0.012 | 0.005 | 0.013 | 0.014 | 0.010 | 0.013 | 0.006 |
| Sum | 0.022 | 0.037 | 0.031 | 0.052 | 0.032 | 0.030 | 0.042 | 0.021 |

TABLE VI.　Systematic uncertainties for $s_i$.

| | $s_1$ | $s_2$ | $s_3$ | $s_4$ | $s_5$ | $s_6$ | $s_7$ | $s_8$ |
|---|---|---|---|---|---|---|---|---|
| $K_i^{(')}$ statistics error | 0.031 | 0.027 | 0.039 | 0.030 | 0.023 | 0.023 | 0.033 | 0.026 |
| Momentum resolution | 0.018 | 0.035 | 0.023 | 0.033 | 0.023 | 0.022 | 0.022 | 0.018 |
| Efficiency variation | 0.018 | 0.012 | 0.019 | 0.010 | 0.013 | 0.018 | 0.013 | 0.012 |
| Single-tag yields | 0.005 | 0.001 | 0.005 | 0.004 | 0.003 | 0.003 | 0.005 | 0.003 |
| Tag side background | 0.004 | 0.001 | 0.001 | 0.003 | 0.001 | 0.004 | 0.002 | 0.001 |
| $K_S^0 \pi^+ \pi^-$ background | 0.005 | 0.008 | 0.030 | 0.023 | 0.005 | 0.003 | 0.016 | 0.014 |
| $K_L^0 \pi^+ \pi^-$ background | 0.050 | 0.022 | 0.018 | 0.035 | 0.006 | 0.024 | 0.005 | 0.025 |
| Multi-candidate selection | 0.036 | 0.018 | 0.033 | 0.012 | 0.022 | 0.026 | 0.028 | 0.011 |
| Non-$D/\bar{D}$ | 0.005 | 0.003 | 0.004 | 0.005 | 0.005 | 0.005 | 0.003 | 0.002 |
| DCSD | 0.023 | 0.004 | 0.030 | 0.019 | 0.015 | 0.006 | 0.027 | 0.020 |
| Sum | 0.077 | 0.055 | 0.076 | 0.069 | 0.045 | 0.052 | 0.060 | 0.050 |

TABLE VII.  Systematic uncertainties for $c_i'$.

| | $c_1'$ | $c_2'$ | $c_3'$ | $c_4'$ | $c_5'$ | $c_6'$ | $c_7'$ | $c_8'$ |
|---|---|---|---|---|---|---|---|---|
| $K_i^{(')}$ statistics error | 0.009 | 0.014 | 0.011 | 0.013 | 0.009 | 0.012 | 0.017 | 0.008 |
| Momentum resolution | 0.008 | 0.016 | 0.014 | 0.020 | 0.010 | 0.013 | 0.019 | 0.010 |
| Efficiency variation | 0.006 | 0.006 | 0.009 | 0.009 | 0.004 | 0.007 | 0.011 | 0.006 |
| Single-tag yields | 0.005 | 0.007 | 0.007 | 0.007 | 0.003 | 0.005 | 0.006 | 0.007 |
| Tag side background | 0.005 | 0.007 | 0.007 | 0.007 | 0.004 | 0.005 | 0.005 | 0.009 |
| $K_S^0 \pi^+ \pi^-$ background | 0.002 | 0.001 | 0.005 | 0.012 | 0.007 | 0.003 | 0.001 | 0.002 |
| $K_L^0 \pi^+ \pi^-$ background | 0.008 | 0.020 | 0.017 | 0.046 | 0.019 | 0.014 | 0.015 | 0.006 |
| Multi-candidate selection | 0.003 | 0.003 | 0.001 | 0.004 | 0.003 | 0.004 | 0.002 | 0.002 |
| Non-$D/\bar{D}$ | 0.012 | 0.018 | 0.005 | 0.006 | 0.004 | 0.004 | 0.008 | 0.005 |
| DCSD | 0.011 | 0.013 | 0.007 | 0.013 | 0.014 | 0.013 | 0.014 | 0.006 |
| Sum | 0.023 | 0.039 | 0.029 | 0.057 | 0.029 | 0.028 | 0.036 | 0.021 |

estimate this part of the uncertainties by varying the input variables $(K_i^{(')})$ one by one according to their statistical uncertainties, and by making new fits. At the end, we take the quadratic sum of all the variations as the systematic error.

Since our Dalitz-plot binning results in bins with unusual shapes and in some cases very narrow regions (see Fig. 1), the migration of events from one bin to another bin may bias our result. The position of an event in the Dalitz plot depends on its momentum determination. The systematic error associated with momentum resolution is studied by smearing the momentum of each fully simulated event in the Monte Carlo sample 200 times, according to the CLEO detector momentum resolution. The distributions of the results for $(c_i, s_i)$ and $(c_i', s_i')$ are then fitted with Gaussian functions, and the widths of the distributions are taken as the systematic uncertainties.

The systematic uncertainties associated with $K_{S/L}^0 \pi^+ \pi^-$ finding cancel under the assumption that the efficiency systematic uncertainties are uniform across the Dalitz plot. Under this condition Eqs. (8) and (10)–(12) have the same dependence on efficiency. To account for a small nonuniformity, we generate a large number of toy experiments where we randomly distribute the relative efficiency of each bin according to a Gaussian distribution (width is taken to be 0.02—a conservative upper limit on the relative efficiency variation across the Dalitz plot) and repeat this process many times. The widths of the resulting distributions for $(c_i, s_i)$ and $(c_i', s_i')$ are taken as systematic uncertainties.

The systematic uncertainties associated with the single-tag yields are evaluated by repeating the fit with the input values varied by their own uncertainties. Assuming the contributions are uncorrelated, we sum in quadrature to obtain the uncertainties on $(c_i, s_i)$ and $(c_i', s_i')$ due to single-tag yields given in Tables V, VI, VII, and VIII.

The systematic uncertainties due to the estimation of the tag side background are studied mode by mode, and the quadratic sum is given in Tables V, VI, VII, and VIII.

Though we used $\Delta E$ and $M(\pi^+ \pi^-)$ mass sidebands for the tag side backgrounds subtraction, we did not apply any background subtraction for $K_S^0 \pi^+ \pi^-$ signal side, which is believed to be small since we require the decay vertex of $K_S^0$ to be separated from the interaction region with a significance greater than 2 standard deviations. The background level in the $K_S^0 \pi^+ \pi^-$ signal region is estimated

TABLE VIII.  Systematic uncertainties for $s_i'$.

| | $s_1'$ | $s_2'$ | $s_3'$ | $s_4'$ | $s_5'$ | $s_6'$ | $s_7'$ | $s_8'$ |
|---|---|---|---|---|---|---|---|---|
| $K_i^{(')}$ statistics error | 0.030 | 0.028 | 0.037 | 0.026 | 0.022 | 0.025 | 0.034 | 0.028 |
| Momentum resolution | 0.022 | 0.042 | 0.031 | 0.042 | 0.029 | 0.028 | 0.031 | 0.033 |
| Efficiency variation | 0.018 | 0.012 | 0.015 | 0.009 | 0.012 | 0.018 | 0.013 | 0.013 |
| Single-tag yields | 0.005 | 0.001 | 0.005 | 0.003 | 0.004 | 0.003 | 0.004 | 0.003 |
| Tag side background | 0.003 | 0.000 | 0.002 | 0.002 | 0.002 | 0.004 | 0.003 | 0.001 |
| $K_S^0 \pi^+ \pi^-$ background | 0.006 | 0.009 | 0.028 | 0.021 | 0.004 | 0.003 | 0.015 | 0.015 |
| $K_L^0 \pi^+ \pi^-$ background | 0.052 | 0.022 | 0.013 | 0.033 | 0.003 | 0.025 | 0.004 | 0.025 |
| Multi-candidate selection | 0.038 | 0.018 | 0.031 | 0.007 | 0.020 | 0.027 | 0.028 | 0.013 |
| Non-$D/\bar{D}$ | 0.005 | 0.003 | 0.004 | 0.005 | 0.004 | 0.005 | 0.003 | 0.002 |
| DCSD | 0.021 | 0.005 | 0.028 | 0.016 | 0.013 | 0.007 | 0.028 | 0.022 |
| Sum | 0.080 | 0.060 | 0.072 | 0.067 | 0.046 | 0.056 | 0.065 | 0.059 |

from $M(\pi^+\pi^-)$ sidebands. We found there is about a 1.9% background in the signal region. We estimate the background contributions from quantum correlated Monte Carlo samples, then make a new fit with the background subtracted. The differences of the results between the nominal fit and the new fit are taken as the systematic uncertainties.

The systematic uncertainties due to the $K_L^0\pi^+\pi^-$ background shape are considered by repeating the fit assuming the background across the Dalitz plot (with the same normalization as in the nominal fit) is uniform. The uncertainties due to the estimation of the background level are negligible. The systematic uncertainties due to flavor-tagged, $CP$-even tagged, $CP$-odd tagged, and $K_S^0\pi^+\pi^-$ tagged $K_L^0\pi^+\pi^-$ samples are considered separately and summed in quadrature in Tables V, VI, VII, and VIII.

It is possible to select a wrong combination when there are multiple signal candidates in an event, especially for $K_S^0\pi^+\pi^-$ vs $K_{S/L}^0\pi^+\pi^-$ samples, since there are many pions with similar momenta. The systematic uncertainties are studied by applying correction matrices to the yield matrices $M_{ij}$. The corrections are typically 2% (5%) for the $K_S^0\pi^+\pi^-$ vs $K_S^0\pi^+\pi^-$ ($K_S^0\pi^+\pi^-$ vs $K_L^0\pi^+\pi^-$) event samples.

Monte Carlo simulated continuum events are checked for non-$D^0/\bar{D}^0$ backgrounds. No significant peaking background is seen for double-tagged $K_S^0\pi^+\pi^-$ samples. The contributions for $K^+K^-$, $\pi^+\pi^-$, and $K_S^0\eta$ tagged $K_L^0\pi^+\pi^-$ samples are also negligible. For other samples, there are $1\sim2\%$ contributions depending on the tag mode. A systematic study is performed by assuming the background (with the same normalization as in the nominal fit) is uniformly distributed over the Dalitz plot.

For the DCSD effect, we made corrections to $K^-\pi^+$ vs $K_{S,L}^0\pi^+\pi^-$ yields in Sec. IV by using results from Ref. [18]. The systematic uncertainties due to $r$ is negligible since it is precisely measured. The systematic uncertainties due to the strong phase $\delta$ are studied by varying it according to its error. For $K^-\pi^+\pi^0$ and $K^-\pi^+\pi^+\pi^-$ tag modes, there are no relative strong phase measurements, so we consider four cases, $\delta = (0°, 90°, 180°, 270°)$, and take the maximum variations among the four cases as the systematic uncertainty.

The total systematic uncertainties on $(c_i, s_i)$ and $(c'_i, s'_i)$—excluding the systematic uncertainty on $\Delta c_i$ and $\Delta s_i$ that relate the $K_S^0\pi^+\pi^-$ and $K_L^0\pi^+\pi^-$ Dalitz-plot models—are obtained from the quadrature sum of these systematic uncertainties, are shown in Tables V, VI, VII, and VIII.

In the global fit, $\Delta c_i$ and $\Delta s_i$ are constrained using a $\chi^2$ term. The errors on $\Delta c_i$ and $\Delta s_i$ are determined by comparing *BABAR*, Belle, and CLEO II $D^0 \to K_S^0\pi^+\pi^-$

TABLE IX. Fit results for $c_i$ and $s_i$. The first error is statistical, the second error is the systematic uncertainty (excluding $\Delta c_i$, $\Delta s_i$), and the third error is the systematic uncertainty due to $\Delta c_i$ and $\Delta s_i$ that relate the $K_S^0\pi^+\pi^-$ and $K_L^0\pi^+\pi^-$ Dalitz-plot models.

| $i$ | $c_i$ | $s_i$ |
|---|---|---|
| 1 | $0.743 \pm 0.037 \pm 0.022 \pm 0.013$ | $0.014 \pm 0.160 \pm 0.077 \pm 0.045$ |
| 2 | $0.611 \pm 0.071 \pm 0.037 \pm 0.009$ | $0.014 \pm 0.215 \pm 0.055 \pm 0.017$ |
| 3 | $0.059 \pm 0.063 \pm 0.031 \pm 0.057$ | $0.609 \pm 0.190 \pm 0.076 \pm 0.037$ |
| 4 | $-0.495 \pm 0.101 \pm 0.052 \pm 0.045$ | $0.151 \pm 0.217 \pm 0.069 \pm 0.048$ |
| 5 | $-0.911 \pm 0.049 \pm 0.032 \pm 0.021$ | $-0.050 \pm 0.183 \pm 0.045 \pm 0.036$ |
| 6 | $-0.736 \pm 0.066 \pm 0.030 \pm 0.018$ | $-0.340 \pm 0.187 \pm 0.052 \pm 0.047$ |
| 7 | $0.157 \pm 0.074 \pm 0.042 \pm 0.051$ | $-0.827 \pm 0.185 \pm 0.060 \pm 0.036$ |
| 8 | $0.403 \pm 0.046 \pm 0.021 \pm 0.002$ | $-0.409 \pm 0.158 \pm 0.050 \pm 0.002$ |

TABLE X. Fit results for $c'_i$ and $s'_i$. The first error is statistical, the second error is the systematic uncertainty (excluding $\Delta c_i$, $\Delta s_i$), and the third error is the systematic uncertainty due to $\Delta c_i$ and $\Delta s_i$.

| $i$ | $c'_i$ | $s'_i$ |
|---|---|---|
| 1 | $0.840 \pm 0.037 \pm 0.023 \pm 0.014$ | $-0.021 \pm 0.160 \pm 0.080 \pm 0.036$ |
| 2 | $0.779 \pm 0.071 \pm 0.039 \pm 0.008$ | $-0.069 \pm 0.215 \pm 0.060 \pm 0.047$ |
| 3 | $0.250 \pm 0.063 \pm 0.029 \pm 0.102$ | $0.587 \pm 0.190 \pm 0.072 \pm 0.006$ |
| 4 | $-0.349 \pm 0.101 \pm 0.057 \pm 0.092$ | $0.275 \pm 0.217 \pm 0.067 \pm 0.058$ |
| 5 | $-0.793 \pm 0.049 \pm 0.029 \pm 0.036$ | $-0.016 \pm 0.183 \pm 0.046 \pm 0.042$ |
| 6 | $-0.546 \pm 0.066 \pm 0.028 \pm 0.038$ | $-0.388 \pm 0.187 \pm 0.056 \pm 0.072$ |
| 7 | $0.475 \pm 0.074 \pm 0.036 \pm 0.081$ | $-0.725 \pm 0.185 \pm 0.065 \pm 0.058$ |
| 8 | $0.591 \pm 0.046 \pm 0.021 \pm 0.011$ | $-0.374 \pm 0.158 \pm 0.059 \pm 0.054$ |

Dalitz-plot fit results. The constraint on $c$ and $c'$ can be removed with little impact on the result. The constraint on $s$ and $s'$ can be relaxed to a factor of 4, but cannot be removed entirely, otherwise, the fit does not converge. To assess our sensitivity to this constraint we consider the following: (1) we relax the constraint by a factor of 2, i.e. increase the errors by a factor of 2 and refit the data; and (2) we fix $\Delta c_i$ and $\Delta s_i$ and refit the data (see Table III). The maximum difference for each $(c_i, s_i)$ and $(c'_i, s'_i)$ between these fits and the nominal fit is interpreted as the systematic uncertainty. An alternate assessment of this systematic uncertainty is the difference in quadrature of the errors reported for the "fixed" and "constrained" fits reported in Table III. The quadrature average of these two methods is reported as the third error on $(c_i, s_i)$ and $(c'_i, s'_i)$ in Table IX and X.

The systematic uncertainties on $c_i$ and $c'_i$ tend to be smaller than the corresponding systematic uncertainty on $s_i$ and $s'_i$. There are two contributing factors: (1) the fact that the $CP$-tagged vs $K^0_{S/L}\pi^+\pi^-$ samples can determine the $c_i$ and $c'_i$, however, these samples provide no constraints on $s_i$ and $s'_i$; and (2) the decay modes with one Dalitz plot ($CP$-tagged vs $K^0_{S/L}\pi^+\pi^-$) have smaller systematic uncertainty than those with two ($K^0_S\pi^+\pi^-$ vs $K^0_{S/L}\pi^+\pi^-$).

## VI. CROSS-CHECK FOR MODEL PREDICTIONS

Using $CP$-tagged $K^0_{S/L}\pi^+\pi^-$ samples, we can get $c_i$ and $c'_i$ without any correlations, so the differences between $c_i$ and $c'_i$ provide a good test of our predictions on the differ-

ences discussed in Sec. II. The comparison between measured $\Delta c_i = c'_i - c_i$ and the *BABAR* model predictions is shown in Fig. 8. We find good agreement between the data and the results obtained using the *BABAR* model, modified to account for the difference between $D^0 \to K^0_S\pi^+\pi^-$ and $D^0 \to K^0_L\pi^+\pi^-$.

## VII. FINAL RESULTS AND IMPACT ON $\gamma/\phi_3$ MEASUREMENT

Our final results for $c_i$, $s_i$, $c'_i$, and $s'_i$ are shown in Fig. 9, Tables IX and X, respectively. The statistical uncertainties dominate for $c_i$ and $s_i$. The systematic uncertainty due to $\Delta c_i$ and $\Delta s_i$ which relate the strong phase difference of $D^0 \to K^0_S\pi^+\pi^-$ and $D^0 \to K^0_L\pi^+\pi^-$ is comparable to all other contributions to the total systematic uncertainty.

To see the impact of our results on the $\gamma/\phi_3$ measurement, we generate toy Monte Carlo $B^\pm \to \tilde{D}^0 K^\pm$ samples with $\gamma/\phi_3 = 60°$, $\delta_B = 130°$, and $r_B = 0.1$. The $B^\pm \to \tilde{D}^0 K^\pm$ sample is large enough so that the statistical uncertainty associated with $B$ decays is negligible. We assume the reconstruction efficiency is 100% and that no background is present. We fit for $\gamma/\phi_3$, $\delta_B$, and $r_B$ 10 000 times by sampling $c_i$ and $s_i$ according to their uncertainties and correlations. We consider the full statistical correlation matrix with (1) uncorrelated, (2) $c_i$ and $s_i$ with fully correlated, and (3) $c_i$ and $s_i$ with fully anticorrelated systematic uncertainties. For (1), we find the width of the resulting $\gamma/\phi_3$ distribution, shown in Fig. 10, is 1.66°. For (2) and (3), the width of the resulting $\gamma/\phi_3$ distribution is
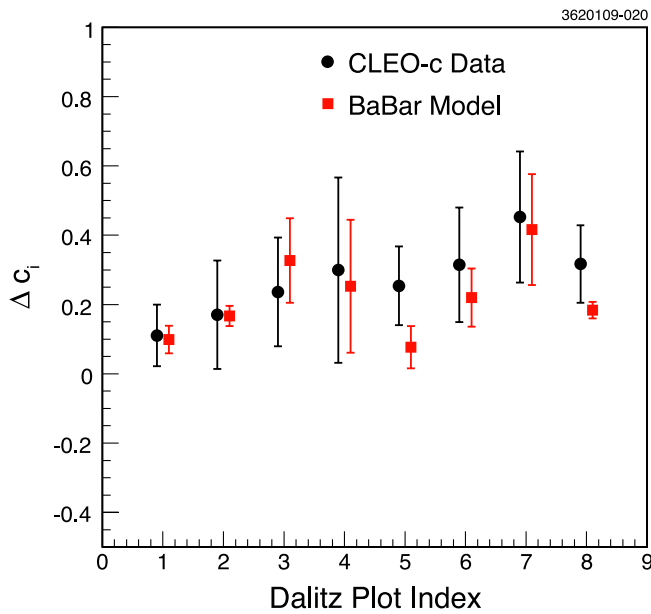


FIG. 8 (color online).   Comparison of $\Delta c_i = c'_i - c_i$ between $CP$-tagged $K^0_{S/L}\pi^+\pi^-$ CLEO-c data (circles) and predictions from the *BABAR* model (squares).
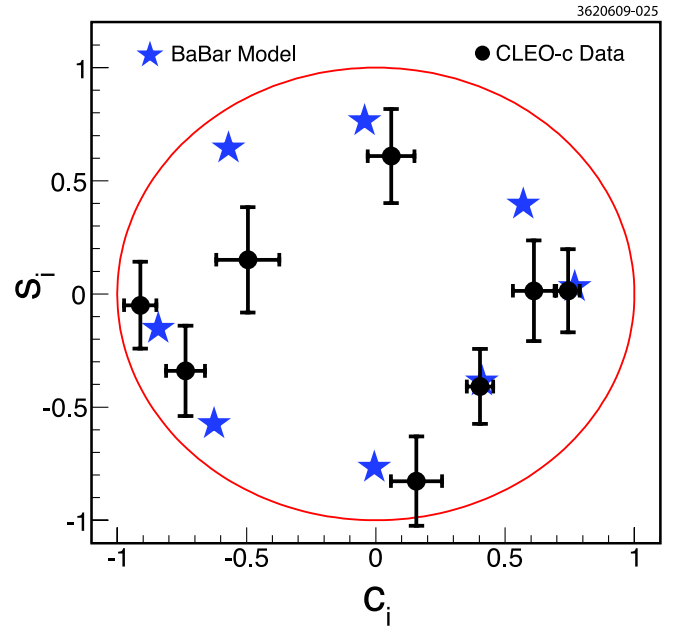


FIG. 9 (color online).   Comparison of $c_i$ and $s_i$ from the nominal fit to CLEO-c data (circles with error bars) presented in Table IX and predictions from the *BABAR* model (stars) presented in Table I.
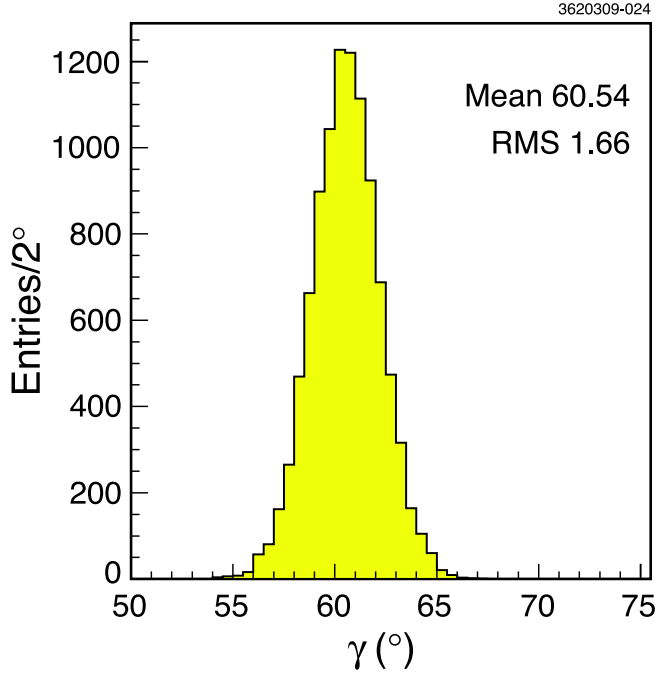
3620309-024



FIG. 10 (color online).   Toy Monte Carlo fit results for $\gamma/\phi_3$.

1.7° and 1.6°, respectively. A small bias of 0.5° is observed, which is caused by the unphysical $c_i$ and $s_i$ pairs (5732 out of 80 000) with $c_i^2 + s_i^2 > 1$. This corresponds to $(7.2 \pm 0.1)\%$. Excluding these bins from the fit reduces the bias to 0.2° which is still significant given the large sample size. However, if we reduce the uncertainties on $c_i$ and $s_i$ by a factor 3 only very few generated bins ( $\ll 1\%$) have unphysical $c_i^2 + s_i^2$ and the distributions of $c_i$ and $s_i$ are Gaussian distributed within the physical region. In this case there is no bias. Therefore, the observed bias is either due to non-Gaussian distributions truncated at the physical boundary or nonphysical values of $c_i^2 + s_i^2$.

Comparing with a model uncertainty of 7° for *BABAR* [7] and 9° for Belle [8], great improvement on the $\gamma/\phi_3$ measurement can be achieved by using a model-independent approach incorporating CLEO-c's results on the strong phase parameters $c_i$ and $s_i$ presented in this article. This will be realized at LHCb where using 10 fb$^{-1}$ of data a *statistical* error on $\gamma/\phi_3$ of 5.5° is

anticipated [9]. The weight of $B \to \tilde{D}K$, $\tilde{D} \to K_S^0 \pi^+ \pi^-$ in the combination of tree-level $\gamma$ measurements at LHCb, which is predicted to have sensitivity of 1°–2° [23], depends upon the CLEO-c's results on the strong phase parameters $c_i$ and $s_i$ presented in this article.

Sensitivity to new physics is obtained through the comparison of $\gamma/\phi_3$ measured directly in tree-level processes and indirect determinations of $\gamma/\phi_3$. One indirect determination, $\gamma/\phi_3 = (67^{+5}_{-4})°$, arises from the intersection of the $B_{(s)}$ mixing and $\sin 2\beta$ contours in the $(\bar{\rho}, \bar{\eta})$ plane [24]. The uncertainty is dominated by the LQCD calculations for mixing [25] and is expected to improve. Another determination of $\gamma/\phi_3$ follows from the unitarity constraint $\gamma = 180° - \alpha - \beta = (70^{+6}_{-5})°$. Here the uncertainty is dominated by the determination of $\alpha/\phi_2 = (88^{+6}_{-5})°$ from $B \to \pi\pi, \rho\pi, \rho\rho$ [24].

## VIII. SUMMARY

In summary, using 818 pb$^{-1}$ of $e^+ e^-$ collisions produced at the $\psi(3770)$, we make a first determination of the strong phase parameters $c_i$ and $s_i$ in Table IX. From a toy Monte Carlo study with a large sample of $B^\pm \to \tilde{D}^0 K^\pm$ data generated with $\gamma/\phi_3 = 60°$, $\delta_B = 130°$, and $r_B = 0.1$, we find that the decay model uncertainty on $\gamma/\phi_3$ is reduced to about 1.7° due to these new measurements. As a result, the precision of the $\gamma/\phi_3$ measurement using $B^+ \to \tilde{D}^0 K^+$ decays will not be limited by the strong interference effects in the $\tilde{D}^0 \to K_S^0 \pi^+ \pi^-$ decay. The improved precision in the direct determination of $\gamma/\phi_3$ enabled by this measurement of the strong phase parameters $c_i$ and $s_i$ enhances sensitivity to new physics through the comparison with indirect determinations of $\gamma/\phi_3$.

## ACKNOWLEDGMENTS

[1] N. Cabibbo, Phys. Rev. Lett. **10**, 531 (1963); M. Kobayashi and T. Maskwaa, Prog. Theor. Phys. **49**, 652 (1973).

[2] A. Giri, Y. Grossman, A. Soffer, and J. Zupan, Phys. Rev. D **68**, 054018 (2003).

[3] Y. Grossman, A. Soffer, and J. Zupan, Phys. Rev. D **72**, 031501 (2005).

[4] See review on $D^0 - \bar{D}^0$ mixing by D. Asner on p. 783–789 of Ref. [15].

[5] D. M. Asner *et al.* (CLEO Collaboration), Phys. Rev. D **70**, 091101 (2004).

[6] B. Aubert *et al.* (*BABAR* Collaboration), Phys. Rev. Lett. **95**, 121802 (2005).

[7] B. Aubert *et al.* (*BABAR* Collaboration), Phys. Rev. D **78**,

034023 (2008).

[8] A. Poluektov *et al.* (Belle Collaboration), Phys. Rev. D **70**, 072003 (2004); **73**, 112009 (2006); K. Abe *et al.* (Belle Collaboration), arXiv:0803.3375.

[9] J. Libby, Report No. CERN-LHCB-2007-141, http://cdsweb.cern.ch/record/1069971?ln=en (unpublished).

[10] A. Bondar *et al.*, Eur. Phys. J. C **47**, 347 (2006); A. Bondar and A. Poluektov, Eur. Phys. J. C **55**, 51 (2008).

[11] H. Muramatsu *et al.* (CLEO Collaboration), Phys. Rev. Lett. **89**, 251802 (2002).

[12] Y. Kubota *et al.* (CLEO Collaboration), Nucl. Instrum. Methods Phys. Res., Sect. A **320**, 66 (1992); D. Peterson *et al.*, Nucl. Instrum. Methods Phys. Res., Sect. A **478**, 142 (2002); M. Artuso *et al.*, Nucl. Instrum. Methods Phys. Res., Sect. A **554**, 147 (2005).

[13] S. Dobbs *et al.* (CLEO Collaboration), Phys. Rev. D **76**, 112001 (2007).

[14] T. E. Coan *et al.* (CLEO Collaboration), Phys. Rev. Lett. **95**, 181802 (2005).

[15] C. Amsler *et al.* (Particle Data Group), Phys. Lett. B **667**, 1 (2008).

[16] S. Kopp *et al.* (CLEO Collaboration), Phys. Rev. D **63**, 092001 (2001).

[17] J. Adler *et al.* (Mark III Collaboration), Phys. Rev. Lett. **62**, 1821 (1989).

[18] J. L. Rosner *et al.* (CLEO Collaboration), Phys. Rev. Lett. **100**, 221801 (2008); D. Asner *et al.* (CLEO Collaboration), Phys. Rev. D **78**, 012001 (2008).

[19] H. Albrecht *et al.* (ARGUS Collaboration), Phys. Lett. B **241**, 278 (1990).

[20] D. Besson *et al.* (CLEO Collaboration), arXiv:0906.2983 [Phys. Rev. D (to be published)].

[21] Q. He *et al.* (CLEO Collaboration), Phys. Rev. Lett. **100**, 091801 (2008).

[22] J. M. Link *et al.* (Focus Collaboration), Phys. Rev. D **75**, 052003 (2007).

[23] K. Akiba *et al.*, Report No. CERN-LHCb-2008-031, http://cdsweb.cern.ch/record/1117819?ln=en (unpublished).

[24] A. Höcker *et al.* (CKMfitter Group), Eur. Phys. J. C **21**, 225 (2001); J. Charles *et al.* (CKMfitter Group), Eur. Phys. J. C **41**, 1 (2005), and updates at http://ckmfitter.in2p3.fr/.

[25] M. Wingate *et al.* (HPQCD Collaboration), Phys. Rev. Lett. **92**, 162001 (2004); A. Gray *et al.* (HPQCD Collaboration), Phys. Rev. Lett. **95**, 212001 (2005); C. Bernard *et al.* (Fermilab Lattice and MILC Collaborations), Proc. Sci., LAT2007 (2007) 370.S. Aoki *et al.* (JLQCD Collaboration), Phys. Rev. Lett. **91**, 212001 (2003); V. Gadiyak and O. Loktik, Phys. Rev. D **72**, 114504 (2005); N. Tantalo, arXiv:hep-ph/0703241.